JGR Oceans

RESEARCH ARTICLE
10.1029/2022JC018948

The Relationship Between Nitrate and Potential Density in the Ocean South of 30°S

Dan Xu[1,2], Tao Wang[1], Xiaogang Xing[3], and Changwei Bian[4]

[1]Key Laboratory of Marine Environment and Ecology, Ocean University of China, Qingdao, China, [2]College of Oceanic and Atmospheric Sciences, Ocean University of China, Qingdao, Shandong, China, [3]State Key Laboratory of Satellite Ocean Environment Dynamics, Second Institute of Oceanography, Ministry of Natural Resources, Hangzhou, China, [4]Frontiers Science Center for Deep Ocean Multispheres and Earth System (FDOMES) and Physical Oceanography Laboratory, Ocean University of China, Qingdao, China

Abstract As a main source of nitrate for the pycnocline in the global ocean, the ocean south of 30°S plays a pivotal role in the global marine biogeochemical cycle. Nitrate in the pycnocline often shows a more stable relationship with density than with depth. Hence, it is important to understand the nitrate structure and its relationship with density in the ocean south of 30°S. In the present study, the nitrate-density relationship and the mechanisms for its variability are studied based on the data from more than 60,000 profiles. Through analysis, we find that nitrate is approximately linearly correlated with potential density in the nitracline, except for the western boundary current zones. The upper bounds of the nitracline depend on the mixed layer and euphotic layer depth. The lower bounds are related to the depth of maximum nitrate, which mainly vary meridionally with sharp changes near the Subantarctic Front. The diapycnal gradients of nitrate also show meridional variability, with large magnitudes corresponding to thick Subantarctic Mode Water, low diapycnal mixing in the nitracline, and high biological uptake in the euphotic layer. The nitrate-density relationship can be applied to predict nitrate concentrations based on the observed temperature and salinity profiles and support some detailed studies on the physical-biogeochemical interactions. Two examples show that the predicted nitrate data could help better resolve the effects of ocean circulations and mesoscale eddies on nitrate than the existing observed nitrate profiles.

Plain Language Summary A high percentage of the global ocean pycnocline nitrate is estimated to originate from the ocean south of 30°S. Nitrate is often found to exhibit a more stable relationship with density than with depth in the pycnocline. Hence, the studies on the nitrate-density relationship in the ocean south of 30°S will not only help understand the transport process of the pycnocline nitrate, but also provide parameters for predicting nitrate concentrations through the observed temperature and salinity, benefiting for the initialization and assimilation of nitrate in ocean models, and the studies those need high-resolution nitrate data. The analysis reveals distinguishing patterns of the nitracline depth and nitrate-density fit slope, both of which show sharp changes near fronts. The large magnitude of nitrate-density fit slope is found to be related to thick Subantarctic Mode Water, low diapycnal mixing under the euphotic layer, and high biological uptake inside the euphotic layer. Given the better spatial and temporal coverage of the observed temperature and salinity profiles, the predicted nitrate data have advantages in resolving more detailed variations of nitrate than the observed nitrate profiles.

Key Points:

- Nitrate and density in the nitracline are approximately linearly related in most regions of the Southern Ocean
- The diapycnal gradients of nitrate in the nitracline are affected by the Subantarctic Mode Water, diapycnal mixing, and biological uptake
- The predicted nitrate field based on the linear-fits helps resolve the effects of mesoscale eddies on the 3-dimensional nitrate distribution

Supporting Information:

Supporting Information may be found in the online version of this article.

Correspondence to:

T. Wang,
taowang@ouc.edu.cn

Citation:

Xu, D., Wang, T., Xing, X., & Bian, C. (2022). The relationship between nitrate and potential density in the ocean south of 30°S. *Journal of Geophysical Research: Oceans*, *127*, e2022JC018948. https://doi.org/10.1029/2022JC018948

Received 7 JUN 2022
Accepted 28 OCT 2022
Corrected 17 DEC 2022

This article was corrected on 17 DEC 2022. See the end of the full text for details.

1. Introduction

In the ocean, dissolved inorganic nitrate (henceforth referred to as nitrate) is one of the essential macronutrients for phytoplankton production. Nitrate is often consumed near the surface by phytoplankton uptake and increases sharply below the euphotic zone through the remineralization of organic matter, exhibiting a strong vertical gradient (here referred to as the nitracline; Omand & Mahadevan, 2015). Physical transport of nitrate across the nitracline is a main nitrogen source for new production in the surface ocean (Ward et al., 1989), which greatly affects the biological activities of phytoplankton, including primary productivity and massive blooms in the euphotic zone (Ardyna et al., 2019; Barocio-León et al., 2007; Johnson & Bif, 2021; Prend et al., 2019; Ryabchenko et al., 1998; Uchida et al., 2019; Wilson et al., 2015), hence the distribution of nitrate inside the nitracline is of particular importance in understanding the biological carbon pump. For instance, in some regions, cold and

windy weather mixes water containing nitrate up to the euphotic zone in the winter. In this way, nitracline plays a significant role in supporting phytoplankton growth the next spring (Martin et al., 2020).

The Southern Ocean is not only the biggest ocean sink region for anthropogenic CO_2 and heat, but also a main source of nutrients for the pycnocline in the global ocean (Fripiat et al., 2021; Watson et al., 2014). A recent study estimates that about 62% of the global ocean pycnocline nitrate and phosphate originate from the Southern Ocean (Fripiat et al., 2021). For instance, with the continuous formation and subduction of the Subantarctic Mode Water (SAMW) originating in the thick wintertime mixed layers, the isopycnal transport of nitrates from the Southern Ocean supports a large amount of nitrate to the upwelling regions of the equatorial Pacific and off South America (Sarmiento et al., 2004). Without the Southern Ocean nutrient source, the sum of the vertical processes that transport nutrients upwards across the pycnocline in the mid- and low-latitude ocean would be insufficient to maintain the biological productivity (Sarmiento et al., 2004). The horizontal transport of nitrate has been proved extremely important for productivity in subtropical circulation oligotrophic systems (Kelly et al., 2021; Letscher et al., 2016; Williams & Follows, 1998). It is foreseeable that the abundant nitrate in the upper seawater of the Antarctic Circumpolar Current (ACC) can be transported to the subtropical oligotrophic basin, according to the northward Ekman transport driven by westerly wind (Manabe et al., 1990). Therefore, studying the distribution of nitrate in the Southern Ocean is key to understanding the sources of the pycnocline nitrate in the global ocean. In some previous studies, the northernmost boundary of the Southern Ocean could extend to nearly 30°S (e.g., Fripiat et al., 2021; Johnson et al., 2017). To include the scope of previous studies and avoid conflict with the concept of the Southern Ocean defined by the National Geographic Society in 2021 (northernmost boundary is 60°S), the area for analysis in the present study is called as the ocean south of 30°S, which is the most inclusive area fully encompassing all Southern Ocean phenomena northward to the Subtropical Front in each ocean.

Various dynamical and biochemical processes in the ocean will affect the distribution of nitrate, resulting in a high degree of variability in the nitrate-depth profiles. Many studies have found that nitrate has a more stable relationship with temperature or density than with depth (e.g., Dugdale et al., 1989; Kamykowski, 1987, 2008; Omand & Mahadevan, 2013; Redfield, 1942; Sarangi et al., 2011), which is inseparable from the fact that large and mesoscale motions in the ocean are often along the isopycnal or isothermal surfaces. Nitrate observations are much fewer and more difficult to measure relative to temperature and salinity. Hence, if the relationship between nitrate and temperature-salinity or density is quantified, much more nitrate data could be derived through the observed temperature and salinity. This will contribute to the initialization and assimilation of nitrate in ocean models, estimation of phytoplankton primary productivity, and studying biogeochemical processes those need high-resolution nitrate data.

To predict nutrient concentrations based on temperature or density in the global or regional oceans, a few studies have applied linear, quadratic, and cubic regression methods to study the nutrients-temperature or nutrients-density relationships (e.g., Dugdale et al., 1997; Garside & Garside, 1995; Holloway, 1986; Kamykowski et al., 2002; Omand et al., 2012; Omand & Mahadevan, 2015; Switzer et al., 2003). In recent years, more approaches have been developed, including artificial neural networks (Możejko & Gniot, 2008), generalized additive models (Primeau et al., 2013), self-organizing maps (Yasunaka et al., 2014), and multiple linear regression (Arteaga et al., 2015). In essence, the fundamental construct of these methods is to establish the relationships between nutrient concentrations and environmental parameters and then predict the unknown nutrient concentrations from known environmental parameters. In general, the environmental parameters associated with the fit of nutrients include temperature, salinity, density, and even dissolved oxygen (Bittig et al., 2018; Sauzède et al., 2017). All of the linear and nonlinear fits have both advantages and disadvantages. Although the multi-order and multi-variable complicated methods could fit a more complex nitrate-density relationship at full depth, the resulted parameters are complicated and usually do not have clear physical or biological significance. It is often hard to find reasonable explanations for the distributions of the complicated parameters based on the oceanic processes. As far as the local nitracline is concerned, the simplest one-order polynomial fit method would reveal its basic features when it satisfies the fit accuracy. Compared with the high-order and machine learning fits, linear-fits have fewer parameters, and the distributions of the parameters are better linked to oceanic processes.

The nitrate-density relationship may vary with space and time (Omand & Mahadevan, 2015). Due to the limitation of the amount of data, previous studies did not propose a relatively high-resolution map that shows clearly the variability of the nitrate-density relationship in the ocean south of 30°S. Biogeochemical-Argo (BGC-Argo), carrying in situ ultraviolet spectrophotometers, can observe the vertical profiles of nitrate with high resolution

Table 1
Number and Period of the Valid Profiles for Analysis in Each Data Set

Data Set	WOD18	BGC-Argo	MGBNPR_015_009
Number of valid profiles	6,885	18,338	37,132
Period	November 1963 to May 2019	February 2008 to May 2022	January 2003 to May 2020

and long time series (Johnson & Coletti, 2002; Johnson et al., 2013), and has been widely used in multidisciplinary studies (e.g., Bittig et al., 2019; Claustre et al., 2020; Johnson et al., 2010; Pellichero et al., 2020; Wang et al., 2021; Xiu & Chai, 2020). In recent years, more and more BGC-Argo floats have been deployed in the ocean south of 30°S, thus providing an opportunity for better understanding the nitrate-density relationship.

In the ocean south of 30°S, nitrate is supposed to be better correlated with density than with depth in the nitracline because physical processes of circulation and mixing dominate the distributions of density and nutrients. The Southern Ocean has a few water masses and fronts, which may have effects on the variability of the nitracline depth and nitrate-density relationship. To characterize the most basic features of the nitrate-density relationship in an effort to gain a mechanistic understanding of the oceanic processes that govern the nitracline shape and depth, linear regression is applied and tested in the present study. The derived nitrate-density relationship is expected to be applied to predict nitrate concentrations in the nitracline based on the observed temperature and salinity data.

2. Data

2.1. Nitrate Profiling Data and Quality Control

The profiles of synchronously measured nitrate concentration, temperature, salinity, and pressure for studying the nitrate-density relationship in the southern area of 30°S are obtained from three data sets, including the World Ocean Database 2018 (WOD18), Biogeochemical Argo (BGC-Argo) data set, and the nutrient estimation data set-MULTIOBS-GLO-BIO-NUTRIENTS-PROFILES-REP-015-009 (MGBNPR_015_009). Potential density is calculated with the temperature, salinity, and pressure by the SeaWater Toolbox (http://www.teos-10.org/).

The WOD18 is provided by the National Centers for Environmental Information (NCEI). The BGC-Argo and Core-Argo profiling data are obtained from https://data-argo.ifremer.fr/ and only adjusted data are used in the present study. The MGBNPR_015_009 data set is downloaded from the Copernicus Marine Service website. It consists of vertical profiles of the concentrations of nitrates, phosphates, and silicates, computed for BGC-Argo equipped with an oxygen sensor from the CANYON (Carbonate system and Nutrients concentration from hydrological properties and Oxygen using a Neural-network) method, first developed by Sauzède et al. (2017) and then improved by Bittig et al. (2018). At the global scale, the nitrate concentration is retrieved with an accuracy (from the root mean squared difference) of 0.68 μmol kg^{-1}.

Before studying the nitrate-density relationship, several data quality-control procedures are performed. First, the profiles without synchronous observations of nitrate concentration, temperature, salinity, and pressure are excluded; Second, we select the data with flag = 0 in WOD18, and the adjusted data with flag = 1 in BGC-Argo and MGBNPR_015_009 data sets for further analysis, in which the accuracy of nitrate concentration is in the order of 10^{-1} μmol kg^{-1}; Third, when the MGBNPR_015_009 data set and the BGC-Argo data set involve the same profiles, only BGC-Argo measured nitrate profiles are used for analysis; Lastly, profiles without nitrate data in the water with depth <30 m are excluded, and the reason is clarified in the Method section. The numbers and periods of the valid profiles from the three data sets after quality control are shown in Table 1. To check the spatial coverage of the profiles, the southern ocean of 30°S is divided into a few 5° × 5° grids. The number of valid profiles for analysis at each grid is shown in Figure 1. There are more than 100 valid profiles in most grids, thus these data are suitable for studying the spatial variability of the nitrate-density relationship to some extent.

2.2. Ancillary Data

To explain the nitrate-density relationship in the ocean south of 30°S, some ancillary data are applied, including the monthly averaged BOA_Argo data set from January 2004 to March 2021 with a horizontal resolution of 1° × 1°, the monthly averaged 3D biogeochemical fields from January 1993 to December 2020 based on the

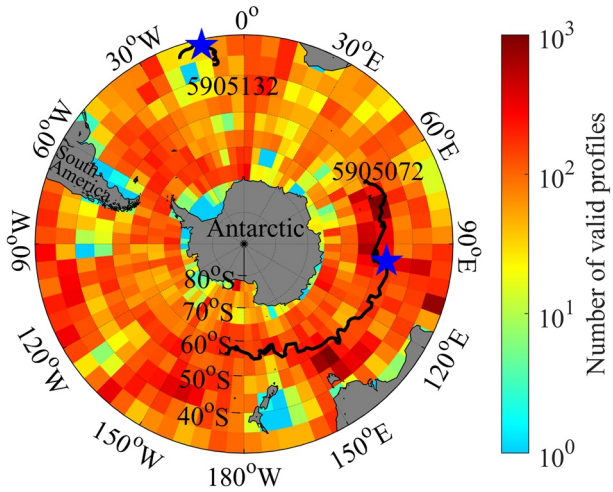

Figure 1. Number of the valid profiles in every 5° × 5° grid. Black lines represent the trajectories of the BGC-Argo floats 5,905,132 and 5,905,072. Blue stars represent the locations of the profiles shown in Figures 2e and 2f.

Pelagic Interactions Scheme for Carbon and Ecosystem Studies (PISCES) biogeochemical model with a horizontal resolution of 0.25° × 0.25° and 75 vertical levels, the monthly averaged euphotic layer depth from September 1997 to August 2021 with a horizontal resolution of 4 × 4 km provided by the GlobColour, gridded sea surface temperature (SST), absolute dynamic topography (ADT) and sea level anomalies (SLA) with a horizontal resolution of 0.25° × 0.25°.

In the present study, mixed layer depth (MLD) is defined as the depth where the potential density has increased from that at 10 m depth by a threshold equivalent to the density difference for the same 0.2°C temperature change at constant salinity (Li et al., 2017). SAMW is defined as the water mass with a threshold ($\Delta Z/\Delta T$ > 75 m °C^{-1}) in the potential density range of 26.5–27.1 kg m^{-3}, temperature range of 0°C–15°C, and salinity range of 34.2–35.8 (Gao et al., 2018). Subantarctic Front (SAF) is defined as the 4°C isotherm at the depth of 400 m according to the criteria of Orsi et al. (1995), which is also the southern boundary of SAMW. South Antarctic Circumpolar Current Front (SACCF) is defined as the 1.8°C isotherm at the depth of 500 m (Orsi et al., 1995), which is corresponding to a strong current in the south of the ACC.

3. Methods

3.1. Linear-Fit Between Nitrate and Density

To explain the fit procedures, the profiles of nitrate concentration observed by the BGC-Argo floats 5,905,132 and 5,905,072 are shown as examples (Figure 2). Their trajectories are around 30°S and 50°S, respectively (Figure 1). As shown in Figure 2, nitrate is consumed near the surface due to the uptake by phytoplankton, increases rapidly with depth in the underlying region through the remineralization of organic matter, and reaches its maximum around 1,000 m. The nitrate profiles observed by these two BGC-Argo floats show that iso-nitrate surfaces are better aligned with the isopycnals than with isobars in the subsurface. In the density coordinate, the lowest potential density has apparent seasonal variability due to the seasonal variations of temperature in the upper layer (Figures 2c and 2d). In the subsurface, isopycnals have little seasonal variability, and the nitrate concentration generally shows less temporal variability along isopycnals (Figures 2c and 2d) than along isobars (Figures 2a and 2b). The vertical profiles from other BGC-Argo floats and WOD18 also show better alignment of iso-nitrate surfaces with isopycnals than isobars (not shown for brevity). Therefore, the relationship between nitrate and density is fitted in this study.

To exclude the surface and deep water, nitracline (fit range) is defined as a bounded region. The upper bound is defined as 2 μmol kg^{-1} larger than the surface nitrate concentration and the lower bound is defined as 1 μmol kg^{-1} smaller than the maximum nitrate concentration in one profile (Figures 2e and 2f). The surface nitrate concentration (N_0) is quantified with the vertically averaged nitrate concentration from surface to 30 m. Thus, profiles without nitrate data above 30 m are excluded in the fit. The definition of the upper bound is similar to the definition of MLD. It differs from that in Omand and Mahadevan (2015), who defined the upper bound as the depth with nitrate concentration of 2 μmol kg^{-1}. In high latitudes, the nitrate-density and nitrate-depth slopes near-surface show distinct features from the underlying water due to mixing and biological uptake inside the euphotic layer, although near-surface nitrate concentration is much higher than 2 μmol kg^{-1} (Figure 2f). Therefore, we define the upper bound as 2 μmol kg^{-1} larger than the surface nitrate concentration.

To characterize the most basic features of the nitrate-density relationship, we apply the simplest linear regression. The coefficients K and B in the linear-fit are obtained through a least squares minimization of

$$NO_{3i} = K\sigma_i + B, i = 1, ...n, \quad (1)$$

where i and n denote each data point and the number of data points in the fit range of one profile, respectively; $\sigma_i = \rho_i - 1{,}000$ kg m^{-3} denotes potential density (herein referred to as density); K denotes the slope of the linear-fit, and B denotes the nitrate intercept.

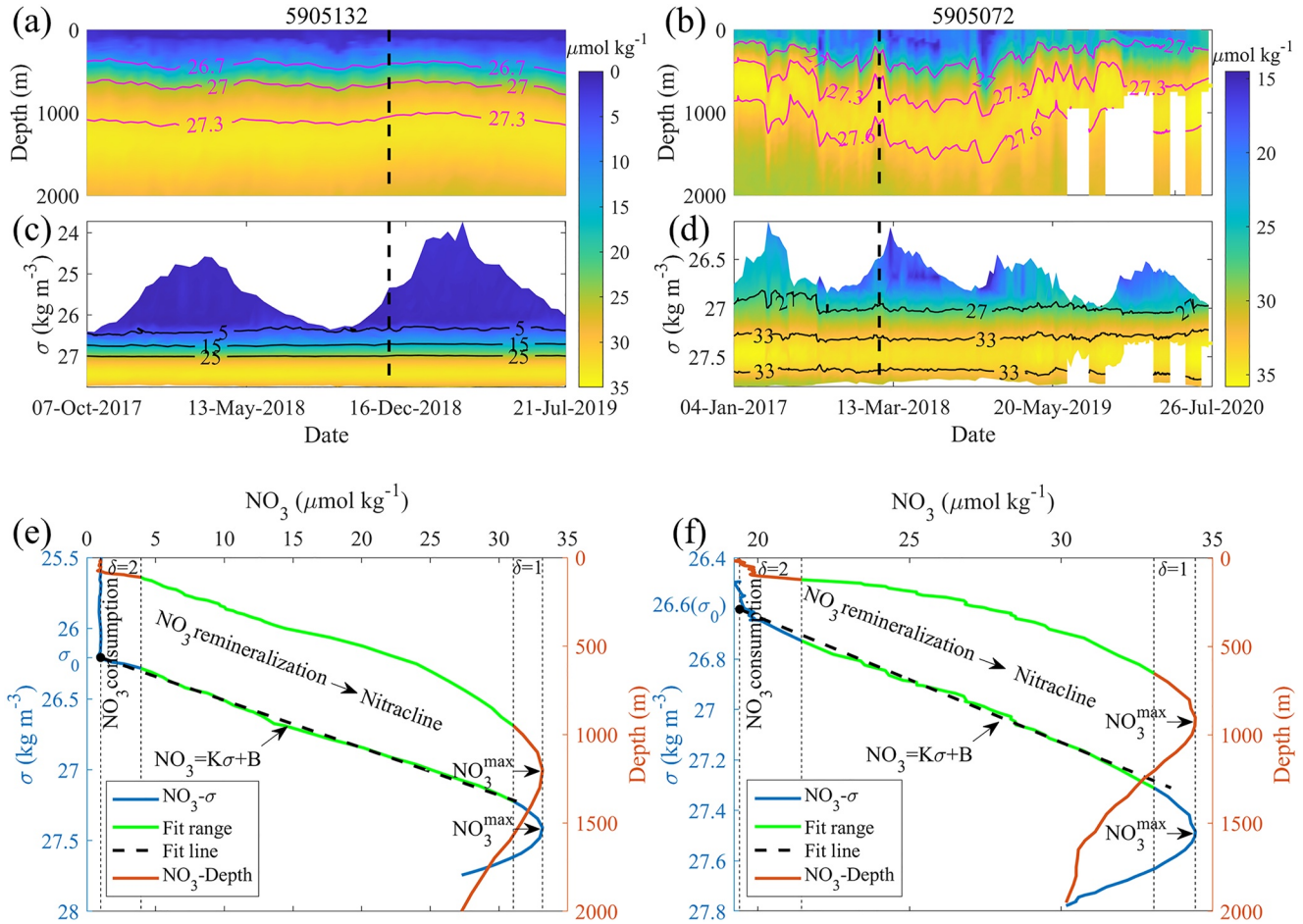

Figure 2. Profiles of nitrate concentration in the depth and density coordinates measured by the BGC-Argo floats 5,905,132 and 5,905,072. In panels (a and b), magenta contours indicate isopycnals. In panels (c and d), black contours indicate iso-nitrate surfaces. Vertical black dashed lines represent the time of the profiles shown in panels (e and f). Panels (e and f) show two typical profiles in the middle and high latitudes, with blue and orange lines representing the variation of nitrate concentration with density and depth, respectively. The green lines represent the bounded region for linear-fit, and the black dash lines represent the fit results.

Nitrate consumption density σ_0 is defined as the density corresponding to the intersection of the fit line and surface nitrate concentration (N_0), which can be written as:

$$\sigma_0 = (N_0 - B)/K. \tag{2}$$

The skill of the fit in each profile is evaluated by:

$$\text{skill} = 1 - \sqrt{\frac{1}{n}\sum_{i=1}^{n}\frac{(\text{NO}_{3i} - \text{NO}_3^{\sigma}(\sigma_i))^2}{\text{NO}_{3i}^2}}. \tag{3}$$

where NO_{3i} and $\text{NO}_3^{\sigma}(\sigma_i)$ denote the observed and fit values of nitrate concentration at each data point, respectively (Omand & Mahadevan, 2015).

3.2. Nitrate-Based Estimation of Annual Net Community Production (ANCP)

To study the effects of biological processes on nitrate, the annual net community production (ANCP) is estimated. Net community production (NCP) is the balance between the primary production of organic matter in the euphotic zone and respiration of that matter by organisms at all trophic levels within the upper ocean. ANCP is the annual integral of NCP, and it is related to the export production and Particulate Organic Carbon in the euphotic zone. We estimate ANCP from the annual drawdown in the surface nitrate reservoir (upper 200 m)

following the method proposed by Arteaga et al. (2019) and Johnson et al. (2017). Nitrate profiles at different latitudes in the ocean south of 30°S show that the seasonal variation of nitrate concentrations is roughly concentrated in the water above 200 m. At depths below 200 m, there is generally good agreement between the summer and winter nitrate profiles (Figure 2; Figure 4 in Johnson et al., 2017). With neglecting the physical processes such as advection and diffusion terms, ANCP can be estimated by converting changes in euphotic zone nutrient inventories to changes in carbon inventories through assuming they are related by Redfield ratios (Munro et al., 2015; Plant et al., 2016). In the present study, based on the outputs from the PISCES biogeochemical model, ANCP is estimated as the vertical integral from the surface to 200 m of the decrease in nitrate concentration (winter maximum month-summer minimum month), converted to carbon units using a Redfield ratio of 106 mol C/16 mol NO_3 (≈6.6):

$$\mathrm{ANCP} = 6.6 \times \int_0^{200} \left[\mathrm{NO}_3^{winter}(z) - \mathrm{NO}_3^{summer}(z)\right] dz. \quad (4)$$

The winter maximum and summer minimum months are identified with the climatologically, monthly and depth averaged nitrate concentration in the upper 200 m. The monthly mean nitrate can also minimize the impact of short-term oscillations in the mixed layer.

4. Results

4.1. Upper and Lower Bounds of Nitracline

The definition of upper bound depth (Z_{upper}), that is, the depth with 2 μmol kg^{-1} greater than the surface nitrate concentration, is similar to the definition of MLD. The magnitude of Z_{upper} roughly reflects the nitrate consumption depth and is influenced by several physical and biological processes, such as vertical mixing, advection, and biological uptake.

As shown in Figure 3, deep Z_{upper} occurs as a ring in the regions between 45°S and 60°S, which is corresponding to the deep annually averaged MLD. The vertical nitrate gradient is very weak due to strong mixing inside the mixed layer and increases rapidly with depth in the nitracline. Thus, the magnitude of Z_{upper} is close to MLD. In the regions between 45°S and 60°S, the strong westerlies results in a relatively uniform mixture of the upper ocean and deeper mixed layer inside the ACC relative to surrounding areas. Therefore, Z_{upper} is deep in the ACC, with a maximum depth nearly 500 m located to the south of Australia (Figure 3a).

The magnitude of Z_{upper} around 30°S is slightly greater than that around 40°S and the South American continent (Figure 3a). This may be related to the effects of the biological uptake depth. Nitrate is consumed by phytoplankton inside the euphotic layer. Through remineralization, nitrate concentration gradually increases below the euphotic layer. Thus the euphotic layer depth (Z_{eu}) is one main factor that determines the deepest depth of the biological uptake. As shown in Figure 3c, the euphotic layer is deeper around 30°S and shallower around 40°S and the South American continent, which is corresponding to the distribution of Z_{upper}. Therefore, the magnitude of Z_{upper} is influenced by the depths of mixed layer and euphotic layer, resulting in similar distribution of Z_{upper} to the maximum of MLD and Z_{eu} (Figure 3d).

The lower bound depth (Z_{lower}) of nitracline, that is, the depth with 1 μmol kg^{-1} smaller than the maximum nitrate concentration, is related to the depth with maximum nitrate concentration. Its spatial distribution mainly shows meridional variability, with sharp changes near SAF (Figure 4a). This is roughly consistent with Omand and Mahadevan (2015). On the north of SAF, the averaged magnitude of Z_{lower} is around 896 m, indicating the deep buried depth of nitrate. On the south of SAF, the upwelling inside the Circumpolar Deep Water (CDW) tilts isopycnals upwards and carries a large amount of nitrate gradually upsurges along isopycnals (Figure 4b), resulting in smaller Z_{lower}, whose average is around 237 m.

4.2. Fit Skill

To test whether linear-fits are appropriate to be applied in the profiles, fit skill is calculated according to Equation 3. The results show that linear-fits are applicable in 91.3% of the profiles ($skill \geq 0.8$). The areas with poor fit skill ($skill < 0.8$) are mainly in the western boundary (warm) current zones, including the Brazil Current, the Agulhas Current, and the East Australia Current zones (Figure 5a).

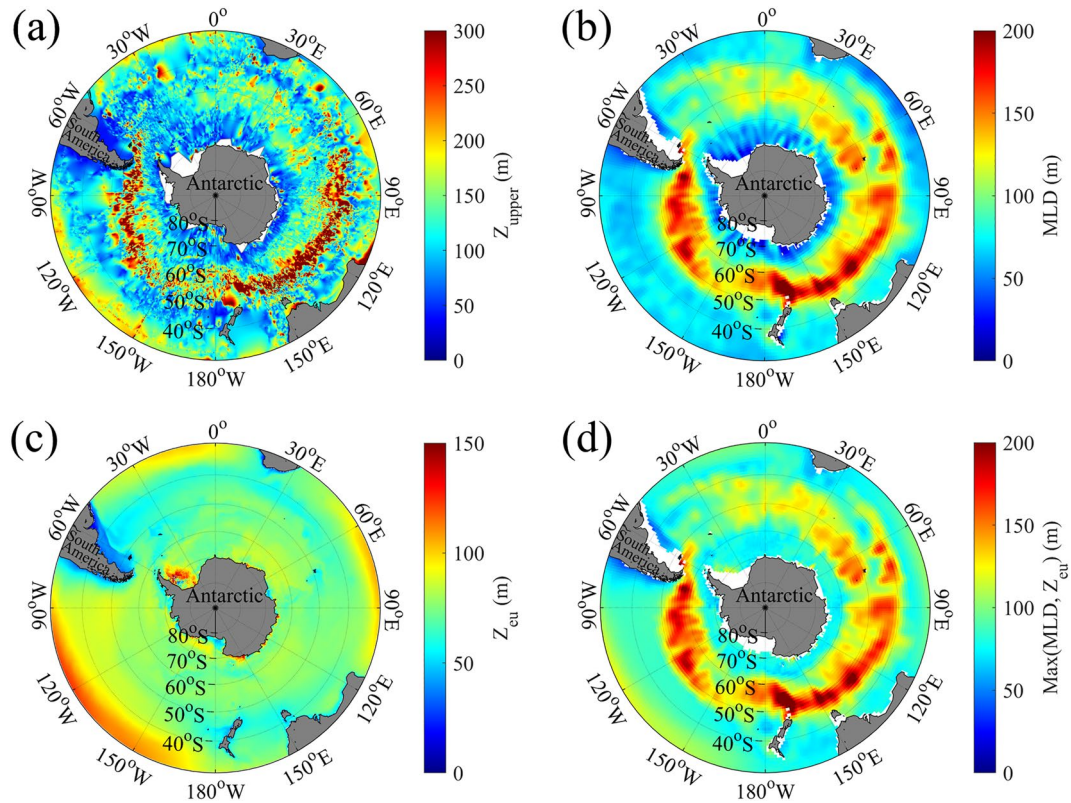

Figure 3. Depth of (a) the upper bound of nitracline, climatologically and annually averaged (b) mixed layer depth (MLD) and (c) euphotic layer depth (Z_{eu}), and (d) maximum of MLD and Z_{eu}.

For comparison, the coefficient of determination of nitrate and density (R^2) is also calculated (Figure 5b), and its average is as high as 0.95. The results of *skill* and R^2 reveal that linear-fits are appropriate to be applied in most regions of the ocean in south of 30°S.

To study the reasons for the poor fit skill in the western boundary current zones, the profiles in the zonal sections across the western boundary current zones are analyzed. The nitrate-density profiles and *T*-*S* diagram in a zonal

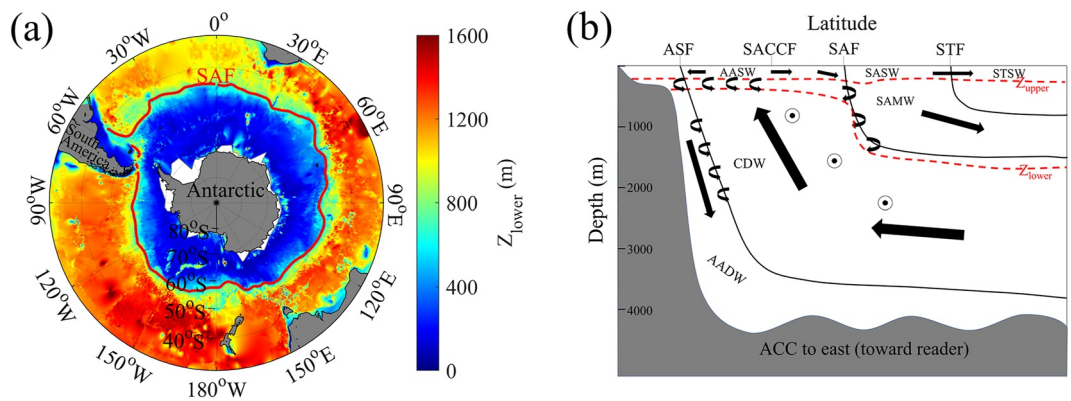

Figure 4. Depth of the lower bound of nitracline and schematic diagram of water masses in the studied area. In panel (a), the red line represents the location of the Subantarctic Front (SAF). Panel (b) shows a schematic meridional section in the ocean south of 30°S, referring to Speer et al. (2000). The area between the red lines represents the bounded region for linear-fit. Acronyms: Antarctic Surface Water (AASW), Subantarctic Mode Water (SAMW), Subantarctic Surface Water (SASW), Subtropical Surface Water (STSW), Antarctic Bottom Water (AADW), Circumpolar Water (CDW), Antarctic Slope Front (ASF), Southern ACC Front (SACCF), Subantarctic Front (SAF), and Subtropical Front (STF).

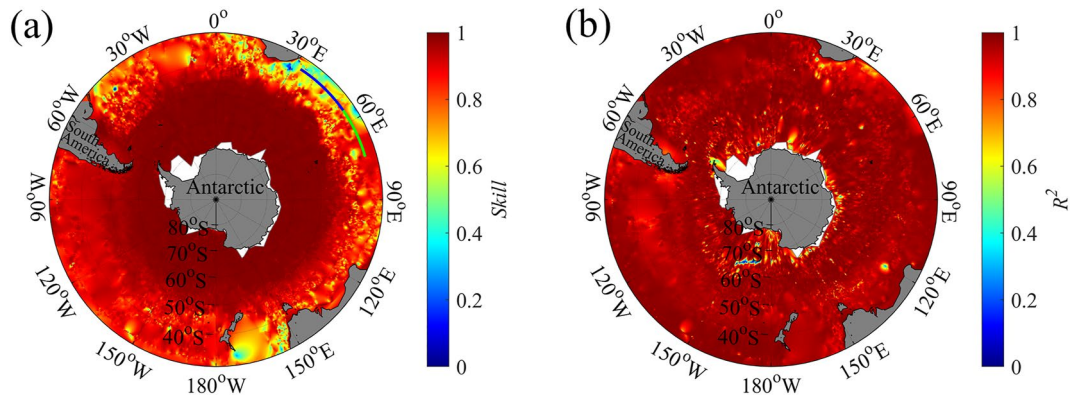

Figure 5. Spatial distributions of (a) linear-fit skill (*skill*) and (b) coefficient of determination (R^2). In panel (a), the blue (33.5°S, 30°–55°E) and green lines (33.5°S, 55°–74°E) represent the sections where profiles are identified with *skill* < 0.8 and *skill* ≥ 0.8, respectively.

section (33.5°S, 30°–74°E) across the Agulhas Current zone are shown in Figure 6 as an example, and the situations in other western boundary current zones are similar.

In the profiles with poor fit skills, the slopes of the upper parts of the nitrate-density lines are obviously inconsistent with the lower parts (Figure 6a), resulting in a low linear-fit skill. As shown in the *T-S* diagram, the thermohaline properties of the profiles with *skill* < 0.8 (blue dots) are different from the profiles with *skill* ≥ 0.8 (green dots; Figure 6b). There is a water mass with high temperature (16°C–20°C) and salinity (35.4–35.6) in the profiles with *skill* < 0.8, which is brought by the Agulhas Current from lower latitudes. Hence, the nitrate-density lines in the upper layer have distinct slopes from the lower layer. The dynamical characteristics in the Brazil Current and the Eastern Australia Current are similar to those in the Agulhas Current, so the fit skills in these two regions are also poor.

4.3. Spatial Distribution of K, B, N_0, and σ_0

When analyzing the distributions of the parameters in the linear-fits, we exclude the areas with *skill* < 0.8 to ensure the accuracy of results. The magnitudes of K mainly vary meridionally, with apparent changes near SAF and SACCF (Figure 7a). In general, the magnitude of K is small on the south of SAF and western side of Chile (<30 μmol m^3 kg^{-2}). In the regions between 40°S and 55°S, the magnitude of K reaches its maximum (generally greater than 40 μmol m^3 kg^{-2}) and rings almost zonally. Due to completely different upper bound in fit, the magnitudes of fit slopes are different from that in Omand and Mahadevan (2015).

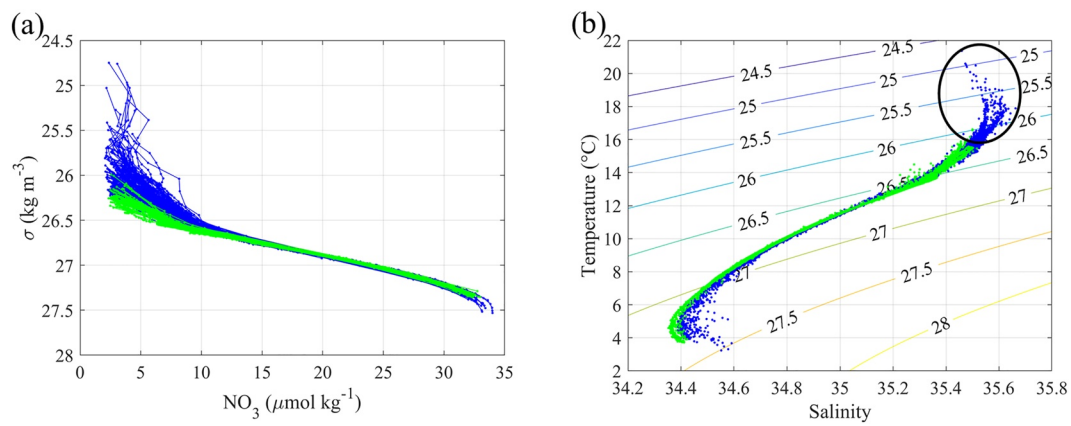

Figure 6. Nitrate-density profiles and *T-S* diagram in a zonal section (33.5°S, 30°–74°E) across the Agulhas Current, whose location is shown in Figure 5a. The blue and green lines represent the profiles with *skill* < 0.8 and *skill* ≥ 0.8, respectively. In panel (b), the green and blue dots correspond to the data points of the blue and green lines in panel (a), respectively.

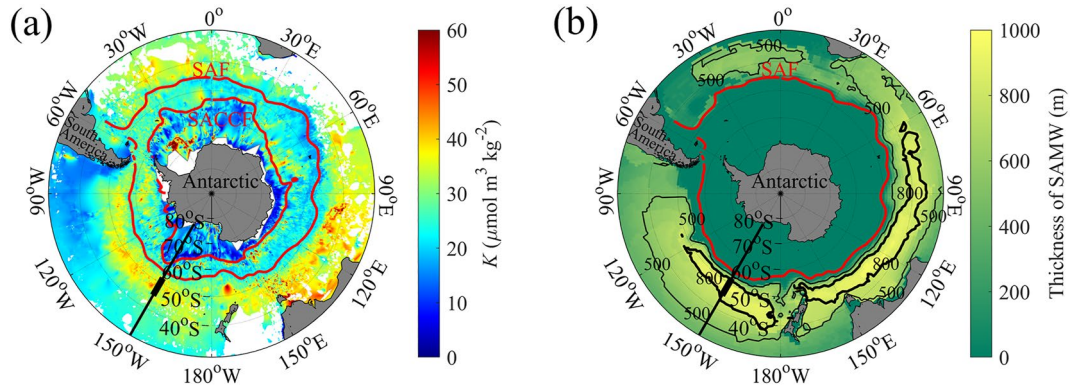

Figure 7. Spatial distributions of (a) K and (b) climatologically and annually averaged thickness of Subantarctic Mode Water (SAMW). The meridional black line (30°–76°S, 150°W) represents the section shown in Figure 9, and the bold part indicates the region with large K (45°–52°S, 150°W). In panel (a), white areas indicate the regions where the linear-fit skills are smaller than 0.8.

The spatial distribution of K is similar to the thickness of SAMW (Figure 7b), with large K corresponding to thick SAMW. The reasons for the correlation between the magnitude of K and the thickness of SAMW are discussed in Section 5. To see whether the seasonality has a significant effect on the magnitude of K, we also calculate the spatial distribution of K in four seasons (Figure S1 in Supporting Information S1). They all show similar patterns as the total result in Figure 7a, indicating that there is no apparent seasonal variability of K. Unlike the WOD18 and BGC-Argo data, the nitrate concentration in the MGBNPR_015_009 data set is not obtained by direct observations. To examine whether the MGBNPR_015_009 data set is appropriate to be applied to study the density-nitrate relationship, we also calculate the spatial distributions of K with only applying this data set and only applying the WOD18 and BGC-Argo data, respectively (Figure S2 in Supporting Information S1). The patterns of K are similar to Figure 7a.

The spatial variation of B (Figure 8a) is opposite to that of K (Figure 7a), with large values of B corresponding to small values of K. The surface nitrate concentration (N_0) is greater than 20 μmol kg^{-1} on the south of SAF and diminishes on the north of 40°S (Figure 8b), so SAF roughly marks the transition from nitrate-limited to nitrate-replete conditions for phytoplankton growth. The nitrate depletion density σ_0, calculated from K, B, and N_0, is close to the deepest isopycnal surface where nitrate is consumed, as shown in Figures 2e and 2f. It generally shows meridional variability, which increases from low to high latitudes (Figure 8c). Since the amount of nitrate

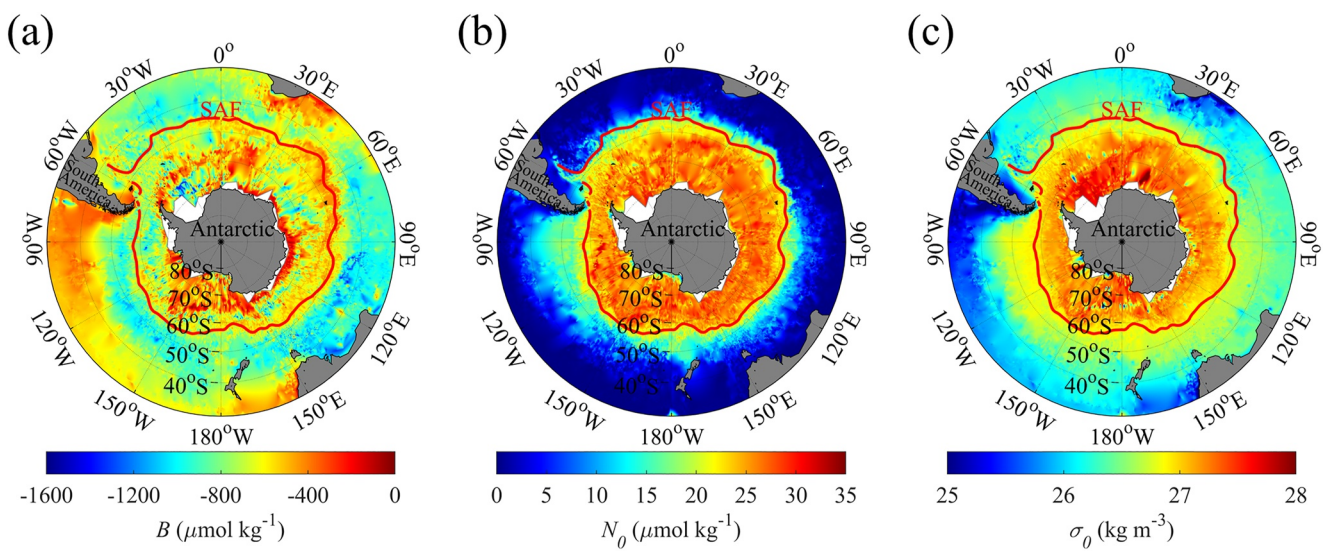

Figure 8. Spatial distributions of (a) nitrate intercept B, (b) surface nitrate concentration N_0 (vertical average in 0–30 m), (c) and nitrate consumption density σ_0.

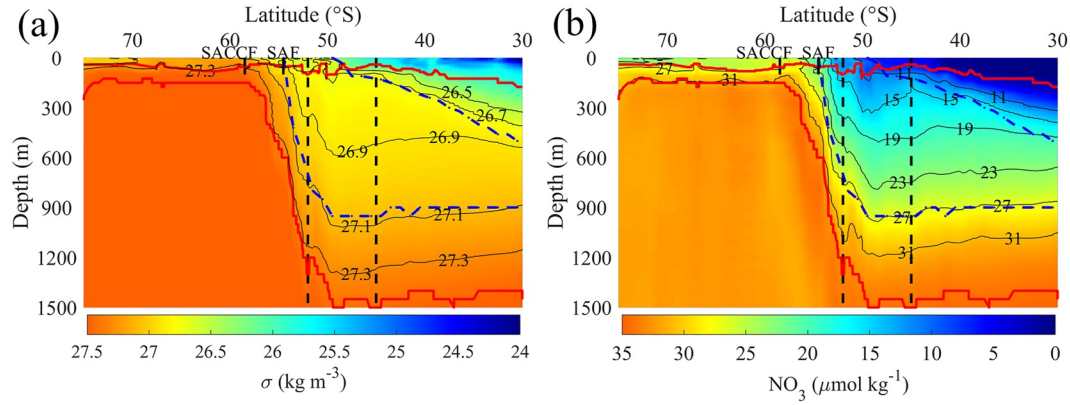

Figure 9. Meridional sections of (a) density and (b) nitrate concentration along 150°W. The region between the blue dotted lines represent Subantarctic Mode Water (SAMW). The red lines represent the upper and lower bounds of the fits. The region with large magnitude of K is shown between the two vertical black dotted lines.

sampling is much smaller than temperature and salinity, it is feasible to derive roughly the deepest depth where nitrate is consumed through known temperature and salinity according to σ_0. It is expected to contribute to some biogeochemical studies, such as the estimation of ANCP.

5. Discussion

5.1. Effects of Water Masses on K

Many biogeochemical fronts in the Southern Ocean are linked to the presence of various water masses with distinct properties. Near the fronts, vertical property gradients are tilted to become horizontal gradients by the action of vertical motions. The SAF is the northernmost frontal jet that passes through Drake Passage. North of SAF, the winter mixed layers can reach more than 700 m in thickness, McCartney (1977, 1982) first described the totality of these thick mixed layers, giving them the name SAMW. SAMW is a pycnostad (a layer of relatively uniform density) that originates in the thick wintertime mixed layers that ring the Southern Ocean (Herraiz-Borreguero, 2010). It is the conduit of nitrate from the Southern Ocean to the upwelling regions of the equatorial Pacific and off South America (Sarmiento et al., 2004). In the SAMW formation region, isopycnals and iso-nitrates both have a certain degree of sinking (Figure 9). With the continuous formation and subduction of cooling waters, SAMW has more homogeneous thermohaline properties than the surrounding water mass. However, nitrate concentration is not homogeneous due to the remineralization of organic matter in the nitracline that covers the depth of SAMW (Figure 9). As a result, K is generally greater ($K > 30$ μmol m^3 kg^{-2}) in the thicker SAMW regions (thickness >500 m; Figure 7). In the regions with the greatest SAMW thickness (thickness >800 m), nitrate concentration increases from 11 μmol kg^{-1} to 27 μmol kg^{-1} as density changes from 26.7 kg m^{-3} to 27.1 kg m^{-3} (Figure 9), resulting in large magnitude of K (≈40 μmol m^3 kg^{-2}), this is corresponding to the results shown in Figure 7a. On the north of the regions with large magnitude of K, as the thickness of SAMW gradually decreases, the contribution of SAMW to K in the nitracline becomes insignificant, so K gradually decreases.

As a consequence of wind-driven upwelling and mixing, dense CDW rises gradually south of SAF. On the south of SAF, nitracline is mainly inside the CDW. CDW carries a large amount of nitrate to upper layer, so nitrate concentration reaches the maximum in a very thin layer (Figure 9b). Strong mixing inside CDW tends to enhance the diapycnal transport of nitrate, resulting in the decrease of the gradient of nitrate relative to density (the magnitude of K). On the south of SACCF, the magnitude of K reaches its minimum. It is perhaps because of the nitrification (the recycling of organic matter to nitrate) in the Antarctic surface waters, which decreases the nitrate concentration gradient (Smart et al., 2015).

The sections in the Atlantic and Indian Ocean have also been examined, and the results show similar patterns to that of the 150°W section in the Pacific Ocean in Figure 9. Therefore, the spatial variation of K is highly correlated with water masses.

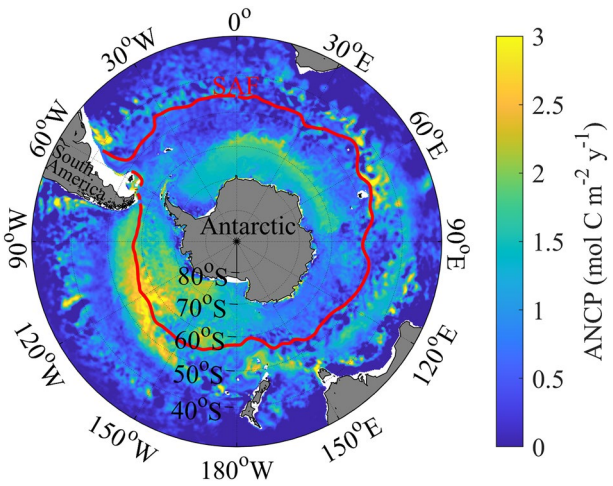

Figure 10. Annual net community production (ANCP) estimated based on nitrate drawdown.

5.2. Effects of Mixing and Biological Processes on *K*

As discussed above, diapycnal mixing and biological processes are perhaps the key factors that determine the difference of *K* in different water masses. Diapycnal mixing inside the nitracline could transport nitrate up across isopycnals and hence decrease the gradient of nitrate relative to density. This can be inferred from the spatial distribution of the turbulence diffusivity (κ_{dia}) across isopycnals in the depth range 300–1,800 m (Figure 1b in Wu et al., 2011). The regions with small magnitudes of *K* (Figure 7a in the present study) are roughly corresponding to the regions with large magnitudes of κ_{dia} (Figure 1b in Wu et al., 2011). Biological uptake consumes nitrate in the euphotic layer, hence has effects on the nitrate concentration at the upper bound for fit. The nitrate concentration at the upper bound will decrease as the biological uptake increases in one profile. This will eventually increase the gradient of nitrate concentration relative to density, so ANCP can affect *K* through biological uptake inside the euphotic layer.

To examine whether the distribution of *K* is related to the biological process, we calculate ANCP according to Equation 4. The magnitude and spatial distribution of ANCP that we obtained agree with the results obtained by Arteaga et al. (2019) (Figure 10), who have verified the consistency of their model results with the results from BGC-Argo data. In the regions with high ANCP (Figure 10), the magnitude of *K* is generally high (Figure 7a). The rough correspondence of ANCP and *K* on the north of SAF indicates that the higher ANCP will lead to larger magnitude of *K* to a certain extent.

Therefore, diapycnal mixing inside the nitracline is in negative correlation with *K*, and ANCP inside the euphotic layer is generally in positive correlation with *K*. Under the combined effects of diapycnal mixing and biological process, high *K* (Figure 7a) is roughly corresponding to low κ_{dia} (Figure 1b in Wu et al., 2011) and high ANCP (Figure 10).

5.3. Prediction of Nitrate Based on the Fit Parameters

Based on the fit parameters, much more nitrate data are expected to be derived from the observed temperature and salinity profiles, which may contribute to the initialization and assimilation of nitrate in ocean models, and studying the physical-biogeochemical interactions those need a large amount of nitrate data. In the areas with fine skills (*skill* ≥ 0.8), we apply the fit parameters to the temperature and salinity profiling data from Core Argo and WOD18 to predict nitrate concentrations in the nitracline. In this section, we present two cases in August 2021 to show how the predicted nitrate concentrations clarify some processes in more details than the existing observed nitrate data.

5.3.1. Filling the Nitrate Observation Gaps

Oceanic currents play primary roles in transporting some oceanic properties (such as temperature and nitrate). Under the effects of large- and mesoscale currents, the isolines of these properties in the upper layer generally tend to be roughly aligned with ADT (Figures 11a and 11b; McGillicuddy, 2016; Wang et al., 2021). However, due to the limited observed nitrate data (193 profiles south of 30°S in August 2021), there appear some apparent mismatches between the isolines of nitrate and SST, such as the regions inside the gray boxes in Figure 11c. The observed temperature and salinity profiles (2,694 profiles south of 30°S in August 2021) are much more than the observed nitrate profiles. The nitrate isolines interpolated from the predicted nitrate data are basically consistent with the results based on the nitrate observations, while they show more similarities with the distributions of ADT and SST in some details (gray boxes in Figure 11d). For instance, on the west of the Antarctic, the isoline of 30 μmol kg^{-1} from the observed nitrate was too further to the west due to very few observed profiles, while the predicted nitrate filled the gaps to some extent. On the southeast of the South America continent, a mesoscale eddy may lead to the curvature of the nitrate isolines. This phenomenon is captured by the predicted nitrate, but not by the observed nitrate data (black box in Figures 11a–11d). The effect of this mesoscale eddy will be discussed in Section 5.3.2.

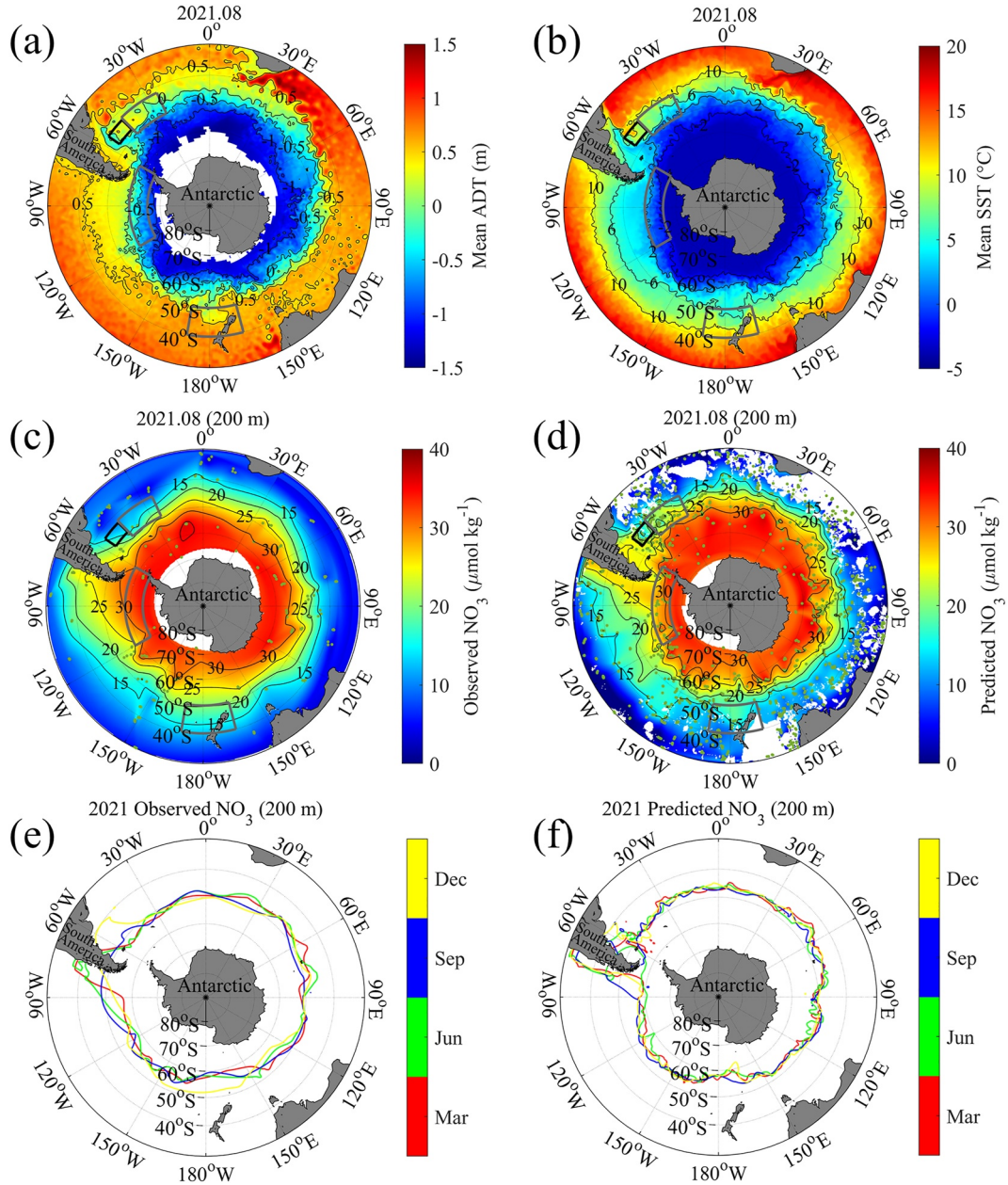

Figure 11. Comparison between the observed and predicted nitrate isolines in August 2021. (a) Monthly averaged ADT; (b) monthly averaged SST; (c) distribution of nitrate concentration at 200 m obtained through interpolating the observed nitrate profiles in August 2021; (d) as (c), but obtained through interpolating the predicted nitrate profiles; (e) isolines of nitrate concentration of 25 μmol kg^{-1} at 200 m obtained through interpolating the observed nitrate profiles in March, June, September, and December 2021; (f) as (e), but obtained through interpolating the predicted nitrate profiles. The nitrate distributions in panels (c–f) are obtained through interpolating the scattered nitrate data linearly in the vertical direction and by the natural neighbor interpolation method in the horizontal direction. In panels (c and d), green dots represent the locations of the profiles for interpolation. The small black rectangular box represents the area in Figure 12.

The nitrate concentration contours at 200 m in different months indicate that there is no apparently seasonal variation in large scales (Figures 11e and 11f). However, the isolines of predicted nitrate are not as smooth as the observed nitrate. This is mainly attributed to the effects of mesoscale meanders and eddies, which is not resolved well by the observed nitrate due to limited profiles.

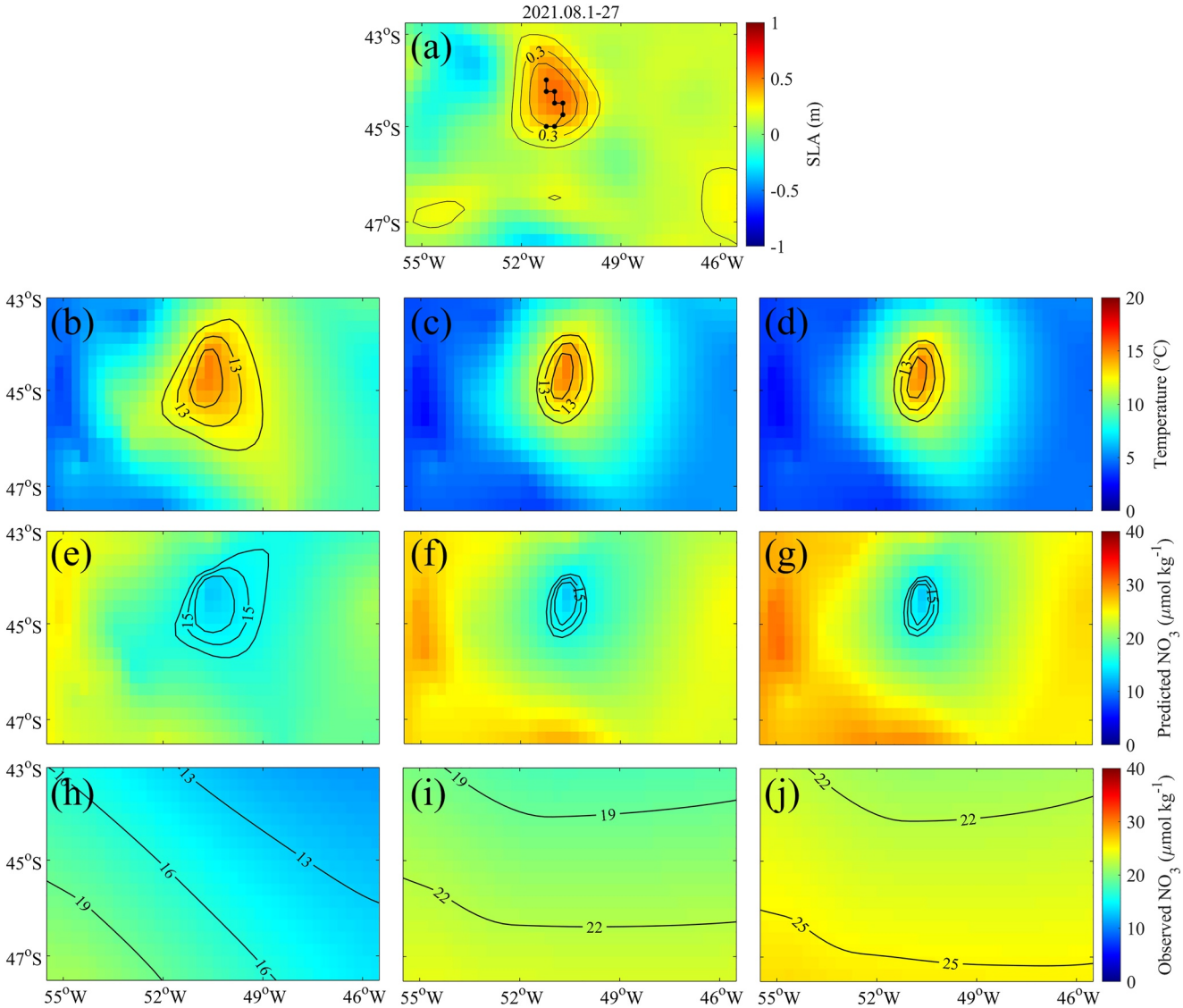

Figure 12. An example that shows the effect of mesoscale eddies on nitrate distribution. (a) Mean Sea Level Anomalies (SLA) from 1 to 27 August in 2021. The black line with dots indicates the trajectory of the eddy center from 1 to 27 August. (b–d) Distributions of temperature at 200, 300, and 400 m interpolated from the observed temperature profiles from 1 to 27 August. (e–g) Distributions of nitrate concentration at 200, 300, and 400 m interpolated from the predicted nitrate profiles from 1 to 27 August. (h–j) As panels (e–g), but interpolated from the observed nitrate profiles. The interpolation method is the same as that in Figures 11c–11f.

5.3.2. Resolving the Effects of Mesoscale Eddies

Mesoscale eddies are ubiquitous and play fundamental roles in physical-biological-biogeochemical interactions in the ocean (McGillicuddy, 2016). Their importance in transporting and redistributing nutrients has been long recognized (e.g., Chen et al., 2020; Ning et al., 2021; Wang et al., 2021), while the existing observed nitrate profiles are not enough to resolve the effects of most eddies. The temperature and salinity profiles are much more than nitrate profiles, and a few studies have applied the Core Argo observed profiles to investigate the effects of mesoscale eddies on heat transport (e.g., Ning et al., 2019; Zhang et al., 2014). Therefore, the predicted nitrate data from temperature and salinity profiles are expected to resolve the effects of mesoscale eddies on nitrate distributions. The mesoscale eddy inside the black box in Figure 11 is analyzed as an example in the following.

In August 2021, an anti-cyclonic mesoscale eddy was generated on the southeast of the South America Continent and moved southward (Figures 11 and 12a). The movement distance of the eddy center from 1 to 27 August was shorter than its diameter (Figure 12a), so the temporal mean SLA from 1 to 27 August was used to show the

averaged location of this eddy. The effect of this eddy on the temperature distribution was well resolved by the temperature profiles during the same time period. The upper warm water converged and sank inside the eddy to induce higher temperature than its surroundings (Figures 12b–12d). The deeper the depth, the smaller diameter of the warm eddy. This was consistent with the three-dimensional structures of mesoscale eddies (Zhang et al., 2014). The predicted nitrate concentrations resolved similar effects of this eddy on nitrate distribution. Due to the sinking induced by this eddy, nitrate concentration was lower inside the eddy than surrounding waters, and the diameter decreased with depth (Figures 12e–12g). In August 2021, there were rarely observed nitrate profiles in the area shown in Figure 12. Thus, the effect of the mesoscale eddy could not be resolved merely by the observed nitrate data (Figures 12h–12j). As discussed above, the predicted nitrate data show some advantages in studying the mesoscale physical-biological-biogeochemical interactions due to their better spatial and temporal coverage than observed nitrate profiles.

Like most predicting models, the prediction based on the linear-fit also has some limitations. First, the linear-fit is based on the data within the nitracline, so it can only be applied within the nitracline. Second, this relationship could not be applied to the areas with $skill < 0.8$, where the fit results do not meet the fit accuracy requirements. Given the pros and cons of the linear and non-linear fit methods, they are expected to be employed to complement each other in future.

6. Conclusions

In the present study, the spatial distributions of nitracline depth, nitrate-density relationship, and their mechanisms in the ocean south of 30°S are investigated. Deep upper bound of the nitracline occurs as a ring in the ACC regions, which is corresponding to the distribution of MLD. The lower bound of nitracline is related to the depth of maximum nitrate concentration, and it shows meridional variability with sharp changes near SAF. The nitrate and density in the nitracline are well correlated and could be fitted linearly in most regions south of 30°S, except for the western boundary current zones. The diapycnal gradient of nitrate, that is, linear-fit slope K, mainly varies meridionally. Its magnitude is related to water masses, diapycnal mixing, and biological uptake. Large magnitudes of K locate in the regions with thick SAMW and roughly correspond to low diapycnal mixing and high ANCP. The nitrate consumption density is close to the deepest isopycnal surface where nitrate is consumed, which also generally shows meridional variability.

These results could help deepen our understanding of the three-dimensional nitrate distribution in the ocean. The diapycnal supply of nitrate to the upper layer depends not only on the transport induced by turbulent mixing, but also on the nitracline depth and diapycnal gradient of nitrate (Omand & Mahadevan, 2015). Lower nitracline depth and larger diapycnal gradient of nitrate are more beneficial for diapycnal nitrate transport when turbulent mixing is the same. Our results portray the nitracline depth and diapycnal gradient of nitrate, helping to assess the diapycnal nitrate flux across the pycnocline and interpret the distribution of primary production in euphotic zone in future studies. In addition, since nutrients and density are often both monotonic continua with respect to depth, they bear a unique relationship to each other, which has been proved to be useful in identifying water mass types (Pytkowicz & Kester, 1966; Redfield, 1942). Through the analysis in the present study, it can be found that the fit results are closely related to the water mass, which is of enlightening significance for the identification of the water mass. One possible idea is to apply the nitrate-density relationship to identify water masses and determine the properties of water bodies in the same way as the temperature-salinity (T-S) diagram. Something similar has already been done (Duarte et al., 2021; Sardessai et al., 2010). Because nitrate is an important nutrient, its content also contains biological information about water mass.

Based on the relatively high-resolution map of the linear-fit parameters, nitrate concentrations are further predicted from the observed temperature and salinity profiles, which are much more than the existing observed nitrate profiles. This is expected to support more detailed studies on the physical-biogeochemical interactions which need better spatial and temporal coverage of nitrate data. Two examples show that the predicted nitrate data could help study the effects of physical processes in more details than the observed nitrate data. For instance, they could help better resolve the effects of ocean circulations and mesoscale eddies on nitrate distributions to some extent, benefiting for studying the mesoscale physical-biogeochemical interactions. In addition, the predicted nitrate concentrations based on density can complement the existing nitrate data sets (Arteaga et al., 2015; Dugdale et al., 1997; Goes et al., 2000; Switzer et al., 2003), which have a few possible practical applications, such as the validation, initialization and assimilation of coupled biological and physical models (Garside & Garside, 1995).

Modeled nitrate data and their relationships with density are expected to fall within reasonable error bounds of the results in the present study. The nitrate-density relationship in the nitracline mainly varies meridionally, indicating that ideally NO_3-σ variability should be mainly meridional in biogeochemical models. This presents the possibility of considerably improving the reproduction of nutrient distributions in biogeochemical models, potentially having a big impact on the model behavior.

In present, although the observed temperature and salinity profiles have been much more than the observed nitrate profiles, they are still not enough to achieve a perfect spatial and temporal coverage. Thus, the predicted nitrate profiles may not be able to fully capture the spatial and temporal variabilities of nitrate concentrations. Nevertheless, the method of predicting nitrate concentration using observed temperature and salinity data has shed light on resolving the effects of mesoscale processes. In future, with the increasing observed profiles, the density-nitrate fits are expected to be more accurate, and the increasing predicted nitrate profiles will help improve our understanding of the physical-biological-biogeochemical interactions in meso- and submeso-scales.

Conflict of Interest

The authors declare no conflicts of interest relevant to this study.

Data Availability Statement

The World Ocean Database 2018 (WOD18) is provided by the National Centers for Environmental Information (NCEI) (https://www.ncei.noaa.gov/products/world-ocean-database). The Biogeochemical-Argo (BGC-Argo) and Core-Argo profiling data are available on the GDAC FTP servers (http://doi.org/10.17882/42182 & ftp://ftp.ifremer.fr/ifremer/argo/). The nutrient estimation data set-MULTIOBS-GLO-BIO-NUTRIENTS-PROFILES-REP-015-009 (MGBNPR_015_009), sea surface temperature (SST), absolute dynamic topography (ADT), and sea level anomalies (SLA) are downloaded from the Copernicus Marine Service website (https://www.copernicus.eu/en). The BOA_Argo data set is downloaded from Argo data products website (https://argo.ucsd.edu/data/argo-data-products/). The 3D biogeochemical fields based on the PISCES (Pelagic Interactions Scheme for Carbon and Ecosystem Studies) biogeochemical model are downloaded from the Copernicus Marine Service website (https://resources.marine.copernicus.eu/product-detail/GLOBAL_MULTIYEAR_BGC_001_029/INFORMATION). The euphotic layer depth (Z_{eu}) data are downloaded from the GlobColour (https://hermes.acri.fr/index.php?class=archive).

Acknowledgments
This study is supported by the Fundamental Research Funds for the Central Universities.

References

Ardyna, M., Lacour, L., Sergi, S., d'Ovidio, F., Sallée, J., Rembauville, M., et al. (2019). Hydrothermal vents trigger massive phytoplankton blooms in the Southern Ocean. *Nature Communications*, *10*(1), 2451. https://doi.org/10.1038/s41467-019-09973-6

Arteaga, L., Pahlow, M., & Oschlies, A. (2015). Global monthly sea surface nitrate fields estimated from remotely sensed sea surface temperature, chlorophyll, and modeled mixed layer depth. *Geophysical Research Letters*, *42*(4), 1130–1138. https://doi.org/10.1002/2014GL062937

Arteaga, L. A., Pahlow, M., Bushinsky, S. M., & Sarmiento, J. L. (2019). Nutrient controls on export production in the Southern Ocean. *Global Biogeochemical Cycles*, *33*(8), 942–956. https://doi.org/10.1029/2019GB006236

Barocio-León, O. A., Millán-Núñez, R., Santamaría-del-Ángel, E., & González-Silvera, A. (2007). Phytoplankton primary productivity in the euphotic zone of the California Current System estimated from CZCS imagery. *Ciencias Marinas*, *33*(1), 59–72. https://doi.org/10.7773/cm.v33i1.1037

Bittig, H. C., Maurer, T. L., Plant, J. N., Schmechtig, C., Wong, A. P. S., Claustre, H., et al. (2019). A BGC-Argo guide: Planning, deployment, data handling, and usage. *Frontiers in Marine Science*, *6*. https://doi.org/10.3389/fmars.2019.00502

Bittig, H. C., Steinhoff, T., Claustre, H., Fiedler, B., Williams, N. L., Sauzède, R., et al. (2018). An alternative to static climatologies: Robust estimation of open ocean CO_2 variables and nutrient concentrations from T, S, and O_2 data using Bayesian neural networks. *Frontiers in Marine Science*, *5*, 328–356. https://doi.org/10.3389/fmars.2018.00328

Chen, K., Gaube, P., & Pallàs-Sanz, E. (2020). On the vertical velocity and nutrient delivery in warm core rings. *Journal of Physical Oceanography*, *50*(6), 1557–1582. https://doi.org/10.1175/JPO-D-19-0239.1

Claustre, H., Johnson, K. S., & Takeshita, Y. (2020). Observing the global ocean with Biogeochemical-Argo. *Annual Review of Marine Science*, *12*(1), 23–48. https://doi.org/10.1146/annurev-marine-010419-010956

Duarte, P., Meyer, A., & Moreau, S. (2021). Nutrients in water masses in the Atlantic sector of the Arctic Ocean: Temporal trends, mixing and links with primary production. *Journal of Geophysical Research: Oceans*, *126*(8), e2021J–e17413J. https://doi.org/10.1029/2021JC017413

Dugdale, R. C., Davis, C. O., & Wilkerson, F. P. (1997). Assessment of new production at the upwelling center at Point Conception, California, using nitrate estimated from remotely sensed sea surface temperature. *Journal of Geophysical Research*, *102*(C4), 8573–8585. https://doi.org/10.1029/96JC02136

Dugdale, R. C., Morel, A., Bricaud, A., & Wilkerson, F. P. (1989). Modeling new production in upwelling centers: A case study of modeling new production from remotely sensed temperature and color. *Journal of Geophysical Research*, *94*(C12), 18119–18132. https://doi.org/10.1029/JC094iC12p18119

Fripiat, F., Martínez-García, A., Marconi, D., Fawcett, S. E., Kopf, S. H., Luu, V. H., et al. (2021). Nitrogen isotopic constraints on nutrient transport to the upper ocean. *Nature Geoscience*, *14*(11), 855–861. https://doi.org/10.1038/s41561-021-00836-8

Gao, L., Rintoul, S. R., & Yu, W. (2018). Recent wind-driven change in Subantarctic Mode Water and its impact on ocean heat storage. *Nature Climate Change*, *8*(1), 58–63. https://doi.org/10.1038/s41558-017-0022-8

Garside, C., & Garside, J. C. (1995). Euphotic-zone nutrient algorithms for the NABE and EqPac study sites. *Deep-Sea Research II*, *42*(2), 335–347. https://doi.org/10.1016/0967-0645(95)00026-M

Goes, J. I., Saino, T., Oaku, H., Ishizaka, J., Wong, C. S., & Nojiri, Y. (2000). Basin scale estimates of sea surface nitrate and new production from remotely sensed sea surface temperature and chlorophyll. *Geophysical Research Letters*, *27*(9), 1263–1266. https://doi.org/10.1029/1999GL002353

Herraiz-Borreguero, L. (2010). *The distribution, circulation, and variability of subantarctic mode water, (Doctoral dissertation)*. University of Tasmania. Retrieved from the University of Tasmania Open Access Repository. https://eprints.utas.edu.au/

Holloway, G. (1986). Estimation of oceanic eddy transports from satellite altimetry. *Nature*, *323*(6085), 243–244. https://doi.org/10.1038/323243a0

Johnson, K. S., & Bif, M. B. (2021). Constraint on net primary productivity of the global ocean by Argo oxygen measurements. *Nature Geoscience*, *14*(10), 769–774. https://doi.org/10.1038/s41561-021-00807-z

Johnson, K. S., & Coletti, L. J. (2002). In situ ultraviolet spectrophotometry for high resolution and long-term monitoring of nitrate, bromide and bisulfide in the ocean. *Deep-Sea Research I*, *49*(7), 1291–1305. https://doi.org/10.1016/S0967-0637(02)00020-1

Johnson, K. S., Coletti, L. J., Jannasch, H. W., Sakamoto, C. M., Swift, D. D., & Riser, S. C. (2013). Long-term nitrate measurements in the Ocean using the in situ ultraviolet spectrophotometer: Sensor integration into the APEX profiling float. *Journal of Atmospheric and Oceanic Technology*, *30*(8), 1854–1866. https://doi.org/10.1175/JTECH-D-12-00221.1

Johnson, K. S., Plant, J. N., Dunne, J. P., Talley, L. D., & Sarmiento, J. L. (2017). Annual nitrate drawdown observed by SOCCOM profiling floats and the relationship to annual net community production. *Journal of Geophysical Research*, *122*(8), 6668–6683. https://doi.org/10.1002/2017JC012839

Johnson, K. S., Riser, S. C., & Karl, D. M. (2010). Nitrate supply from deep to near-surface waters of the North Pacific subtropical gyre. *Nature*, *465*(7301), 1062–1065. https://doi.org/10.1038/nature09170

Kamykowski, D. (1987). A preliminary biophysical model of the relationship between temperature and plant nutrients in the upper ocean. *Deep-Sea Research*, *34*(7), 1067–1079. https://doi.org/10.1016/0198-0149(87)90064-1

Kamykowski, D. (2008). Estimating upper ocean phosphate concentrations using ARGO float temperature profiles. *Deep-Sea Research I*, *55*(11), 1580–1589. https://doi.org/10.1016/j.dsr.2008.05.017

Kamykowski, D., Zentara, S., Morrison, J. M., & Switzer, A. C. (2002). Dynamic global patterns of nitrate, phosphate, silicate, and iron availability and phytoplankton community composition from remote sensing data. *Global Biogeochemical Cycles*, *16*(4), 21–25. https://doi.org/10.1029/2001GB001640

Kelly, T. B., Knapp, A. N., Landry, M. R., Selph, K. E., Shropshire, T. A., Thomas, R. K., & Stukel, M. R. (2021). Lateral advection supports nitrogen export in the oligotrophic open-ocean Gulf of Mexico. *Nature Communications*, *12*(1), 3325. https://doi.org/10.1038/s41467-021-23678-9

Letscher, R. T., Primeau, F., & Moore, J. K. (2016). Nutrient budgets in the subtropical ocean gyres dominated by lateral transport. *Nature Geoscience*, *9*(11), 815–819. https://doi.org/10.1038/ngeo2812

Li, H., Xu, F., Zhou, W., Wang, D., Wright, J. S., Liu, Z., & Lin, Y. (2017). Development of a global gridded Argo data set with Barnes successive corrections. *Journal of Geophysical Research*, *122*(2), 866–889. https://doi.org/10.1002/2016JC012285

Manabe, S., Bryan, K., & Spelman, M. J. (1990). Transient response of a global ocean-atmosphere model to a doubling of atmospheric carbon dioxide. *Journal of Physical Oceanography*, *20*(5), 722–749. https://doi.org/10.1175/1520-0485(1990)020<0722:TROAGO>2.0.CO;2

Martin, A., Boyd, P., Buesseler, K., Cetinic, I., Claustre, H., Giering, S., et al. (2020). Study the twilight zone before it is too late. *Nature*, *28*(7801), 26–28. https://doi.org/10.1038/d41586-020-00915-7

McCartney, M. S. (1977). Subantarctic mode water, in A voyage of discovery. *Deep-Sea Research George Deacon 10th Anniversary*, *103–119*.

McCartney, M. S. (1982). The subtropical recirculation of mode waters. *Journal of Marine Research*, *40*, 427–464.

McGillicuddy, D. J. (2016). Mechanisms of physical-biological-biogeochemical interaction at the oceanic mesoscale. *Annual Review of Marine Science*, *8*(1), 125–159. https://doi.org/10.1146/annurev-marine-010814-015606

Możejko, J., & Gniot, R. (2008). Application of neural networks for the prediction of total phosphorus concentrations in surface waters. *Polish Journal of Environmental Studies*, *17*(3), 363–368.

Munro, D. R., Lovenduski, N. S., Stephens, B. B., Newberger, T., Arrigo, K. R., Takahashi, T., et al. (2015). Estimates of net community production in the Southern Ocean determined from time series observations (2002–2011) of nutrients, dissolved inorganic carbon, and surface ocean pCO2 in Drake Passage. *Deep-Sea Research I*, *114*, 49–63. https://doi.org/10.1016/j.dsr2.2014.12.014

Ning, J., Chen, K., & Gaube, P. (2021). Diverse variability of surface chlorophyll during the evolution of Gulf Stream rings. *Geophysical Research Letters*, *48*, e2020GL091461. https://doi.org/10.1029/2020GL091461

Ning, J., Xu, Q., Zhang, H., Wang, T., & Fan, K. (2019). Impact of cyclonic ocean eddies on upper ocean thermodynamic response to typhoon Soudelor. *Remote Sensing*, *11*, 938. https://doi.org/10.3390/rs11080938

Omand, M. M., Feddersen, F., Guza, R. T., & Franks, P. J. S. (2012). Episodic vertical nutrient fluxes and nearshore phytoplankton blooms in Southern California. *Limnology & Oceanography*, *57*(6), 1673–1688. https://doi.org/10.4319/lo.2012.57.6.1673

Omand, M. M., & Mahadevan, A. (2013). Large-scale alignment of oceanic nitrate and density. *Journal of Geophysical Research*, *118*(10), 5322–5332. https://doi.org/10.1002/jgrc.20379

Omand, M. M., & Mahadevan, A. (2015). The shape of the oceanic nitracline. *Biogeosciences*, *12*(11), 3273–3287. https://doi.org/10.5194/bg-12-3273-2015

Orsi, A. H., Whitworth, T., & Nowlin, W. D. (1995). On the meridional extent and fronts of the Antarctic Circumpolar Current. *Deep-Sea Research I*, *42*(5), 641–673. https://doi.org/10.1016/0967-0637(95)00021-W

Pellichero, V., Boutin, J., Claustre, H., Merlivat, L., Sallée, J. B., & Blain, S. (2020). Relaxation of wind stress drives the abrupt onset of biological carbon uptake in the Kerguelen bloom: A multisensor approach. *Geophysical Research Letters*, *47*(9), e2019GL085992. https://doi.org/10.1029/2019GL085992

Plant, J. N., Johnson, K. S., Sakamoto, C. M., Jannasch, H. W., Coletti, L. J., Riser, S. C., & Swift, D. D. (2016). Net community production at Ocean Station Papa observed with nitrate and oxygen sensors on profiling floats. *Global Biogeochemical Cycles*, *30*(6), 859–879. https://doi.org/10.1002/2015GB005349

Prend, C. J., Gille, S. T., Talley, L. D., Mitchell, B. G., Rosso, I., & Mazloff, M. R. (2019). Physical drivers of phytoplankton bloom initiation in the Southern Ocean's Scotia Sea. *Journal of Geophysical Research*, *124*(8), 5811–5826. https://doi.org/10.1029/2019JC015162

Primeau, F. W., Holzer, M., & DeVries, T. (2013). Southern Ocean nutrient trapping and the efficiency of the biological pump. *Journal of Geophysical Research*, *118*(5), 2547–2564. https://doi.org/10.1002/jgrc.20181

Pytkowicz, R. M., & Kester, D. R. (1966). Oxygen and phosphate as indicators for the deep intermediate waters in the northeast Pacific Ocean. *Deep Sea Research and Oceanographic Abstracts*, *13*(3), 373–379. https://doi.org/10.1016/0011-7471(66)91075-8

Redfield, A. C. (1942). The processes determining the concentration of oxygen, phosphate, and other organic derivatives within the depths of the Atlantic Ocean. *Physical Oceanography and Meteorology*, *9*(2), 1–22. https://doi.org/10.1575/1912/1053

Ryabchenko, V. A., Gorchakov, V. A., & Fasham, M. J. R. (1998). Seasonal dynamics and biological productivity in the Arabian Sea Euphotic Zone as simulated by a three-dimensional ecosystem model. *Global Biogeochemical Cycles*, *12*(3), 501–530. https://doi.org/10.1029/98GB01183

Sarangi, R. K., Thangaradjou, T., Saravanakumar, A., & Balasubramanian, T. (2011). Development of nitrate algorithm for the southwest Bay of Bengal water and its implication using remote sensing satellite data sets. *Ieee Journal of Selected Topics in Applied Earth Observations and Remote Sensing*, *4*(4), 983–991. https://doi.org/10.1109/JSTARS.2011.2165204

Sardessai, S., Shetye, S., Maya, M. V., Mangala, K. R., & Prasanna Kumar, S. (2010). Nutrient characteristics of the water masses and their seasonal variability in the eastern equatorial Indian Ocean. *Marine Environmental Research*, *70*(3), 272–282. https://doi.org/10.1016/j.marenvres.2010.05.009

Sarmiento, J. L., Gruber, N., Brzezinski, M. A., & Dunne, J. P. (2004). High-latitude controls of thermocline nutrients and low-latitude biological productivity. *Nature*, *427*(6969), 56–60. https://doi.org/10.1038/nature02127

Sauzède, R., Bittig, H. C., Claustre, H., Pasqueron de Fommervault, O., Gattuso, J., Legendre, L., & Johnson, K. S. (2017). Estimates of water-column nutrient concentrations and carbonate system parameters in the global ocean: A novel approach based on neural networks. *Frontiers in Marine Science*, *4*. https://doi.org/10.3389/fmars.2017.00128

Smart, S. M., Fawcett, S. E., Thomalla, S. J., Weigand, M. A., Reason, C. J. C., & Sigman, D. M. (2015). Isotopic evidence for nitrification in the Antarctic winter mixed layer. *Global Biogeochemical Cycles*, *29*(4), 427–445. https://doi.org/10.1002/2014GB005013

Speer, K., Rintoul, S. R., & Sloyan, B. (2000). The diabatic deacon cell. *Journal of Physical Oceanography*, *30*(12), 3212–3222. https://doi.org/10.1175/1520-0485(2000)030<3212:TDDC>2.0.CO;2

Switzer, A. C., Kamykowski, D., & Zentara, S. (2003). Mapping nitrate in the global ocean using remotely sensed sea surface temperature. *Journal of Geophysical Research*, *108*(C8). https://doi.org/10.1029/2000JC000444

Uchida, T., Balwada, D., Abernathey, R., Prend, C. J., Boss, E., & Gille, S. T. (2019). Southern Ocean phytoplankton blooms observed by biogeochemical floats. *Journal of Geophysical Research*, *124*(11), 7328–7343. https://doi.org/10.1029/2019JC015355

Wang, T., Chai, F., Xing, X., Ning, J., Jiang, W., & Riser, S. C. (2021). Influence of multi-scale dynamics on the vertical nitrate distribution around the Kuroshio Extension: An investigation based on BGC-Argo and satellite data. *Progress in Oceanography*, *193*, 102543. https://doi.org/10.1016/j.pocean.2021.102543

Ward, B. B., Kilpatrick, K. A., Renger, E. H., & Eppley, R. W. (1989). Biological nitrogen cycling in the nitracline. *Limnology & Oceanography*, *34*(3), 493–513. https://doi.org/10.4319/lo.1989.34.3.0493

Watson, A. J., Meredith, M. P., & Marshall, J. (2014). The Southern Ocean, carbon, and climate. *Philosophical Transactions of the Royal Society A: Mathematical, Physical & Engineering Sciences*, *372*(2019), 20130057. https://doi.org/10.1098/rsta.2013.0057

Williams, R. G., & Follows, M. J. (1998). The Ekman transfer of nutrients and maintenance of new production over the North Atlantic. *Deep-Sea Research I*, *45*(2), 461–489. https://doi.org/10.1016/S0967-0637(97)00094-0

Wilson, S. T., Barone, B., Ascani, F., Bidigare, R. R., Church, M. J., Del Valle, D. A., et al. (2015). Short-term variability in euphotic zone biogeochemistry and primary productivity at Station ALOHA: A case study of summer 2012. *Global Biogeochemical Cycles*, *29*(8), 1145–1164. https://doi.org/10.1002/2015GB005141

Wu, L., Jing, Z., Riser, S., & Visbeck, M. (2011). Seasonal and spatial variations of Southern Ocean diapycnal mixing from Argo profiling floats. *Nature Geoscience*, *4*(6), 363–366. https://doi.org/10.1038/ngeo1156

Xiu, P., & Chai, F. (2020). Eddies affect subsurface phytoplankton and oxygen distributions in the North Pacific subtropical gyre. *Geophysical Research Letters*, *47*(15), e2020G–e87037G. https://doi.org/10.1029/2020GL087037

Yasunaka, S., Nojiri, Y., Nakaoka, S., Ono, T., Whitney, F. A., & Telszewski, M. (2014). Mapping of sea surface nutrients in the North Pacific: Basin-wide distribution and seasonal to interannual variability. *Journal of Geophysical Research*, *119*(11), 7756–7771. https://doi.org/10.1002/2014JC010318

Zhang, Z., Wang, W., & Qiu, B. (2014). Oceanic mass transport by mesoscale eddies. *Science*, *345*(6194), 322–324. https://doi.org/10.1126/science.1252418

References From the Supporting Information

du Plessis, M., Swart, S., Ansorge, I., Mahadevan, A., & Thompson, A. (2019). Southern Ocean seasonal restratification delayed by submesoscale wind-front interactions. *Journal of Physical Oceanography*, *49*(4), 1035–1053. https://doi.org/10.1175/JPO-D-18-0136.1

Erratum

The originally published version of the Supporting Information for this article included an outdated copy of Figure S1. The error has been corrected, and this may be considered the official version of record.